Nuclear Materials and Energy 20 (2019) 100682

Contents lists available at ScienceDirect

Nuclear Materials and Energy

journal homepage: www.elsevier.com/locate/nme

Modeling of H/D isotope-exchange in crystalline beryllium

D. Matveev*, P. Hansen, T. Dittmar, H.R. Koslowski, Ch. Linsmeier

Forschungszentrum Jülich GmbH, Institut für Energie- und Klimaforschung – Plasmaphysik, Partner of the Trilateral Euregio Cluster (TEC), 52425 Jülich, Germany

ARTICLE INFO

Keywords:
Beryllium
Isotope-exchange
Hydrogen retention
Reaction-diffusion
TDS

ABSTRACT

A reaction-diffusion model with surface occupation dependent desorption [D. Matveev et al., Nucl. Instr. Meth. B 430 (2018) 23–30] has been updated to handle multiple hydrogen species to simulate hydrogen/deuterium isotope-exchange experiments performed on polycrystalline beryllium samples under ultra-high vacuum laboratory conditions. In the experiments subsequent exposures of a sample to hydrogen and deuterium ion beams in direct and reverse implantation order were followed by thermal desorption spectroscopy measurements under a constant heating rate of 0.7 K/s. The recorded signals of masses 2 to 4 (H_2, HD and D_2) indicate that the second implanted isotope dominates clearly the low temperature release stage (≈ 450 K), while both isotopes show a comparable contribution to the high temperature desorption stage (≈ 700 K) with only minor effect of the implantation order attributed to a slightly deeper penetration of deuterium compared to hydrogen. Simulations of the implantation and subsequent thermal desorption of hydrogen isotopes are performed to assess the atomic processes behind the isotope-exchange. Simulations were performed under the assumption that the low temperature release stage is attributed to hydrogen/deuterium atoms retained on effective open surfaces (e.g. interconnected porosity) represented in the simulations by a surface with an effective surface area exceeding the nominal exposed surface area by a factor up to 100. Kinetic de-trapping from vacancies with multiple trapping levels and enhanced desorption at surface coverages close to saturation are addressed in the model as possible mechanisms promoting the isotope-exchange. Simulation results suggest the applicability of the model to describe isotope-exchange processes in crystalline beryllium and give a qualitative explanation of the observed experimental facts.

1. Introduction

Understanding the effects of plasma exposure on plasma-facing materials (PFM) is essential for reliable estimates of the wall lifetime, tritium retention and overall plasma performance in a fusion reactor. Beryllium (Be) is selected as PFM for the first wall in ITER. Properties of Be relevant for plasma-wall interactions were reviewed by Federici et al. in [1]. Nevertheless, the mechanisms of retention and release of hydrogen isotopes in metallic beryllium on the atomic scale are still not well understood. These mechanisms govern fuel inventory and recycling, affect physical properties of the material, and represent an interesting fundamental question.

Experiments on the interaction of hydrogen isotopes with metallic Be were performed in the past by several research teams and are reviewed in [2] and [3]. Experiments were performed with deuterium (D) to distinguish it from protium (H) naturally present in the residual gas and as wall adsorbates (mainly water vapor) in the experimental vacuum chamber even under ultra-high vacuum (UHV) laboratory conditions. Chernikov, Markin and Alimov [4–6] implanted Be samples with 3 to 9 keV D ions at room temperature, as well as at elevated temperatures, and analyzed the evolution of D retention and release by means of thermal desorption spectroscopy (TDS) in correlation with the evolution of the microstructure using transmission electron microscopy (TEM). Combining residual gas analysis (RGA) measurements with secondary ion mass spectrometry (SIMS), depth profiles of D retained in atomic and molecular form were deduced. The total D retention increased almost linearly with the exposure fluence, with negligible D re-emission, up to a certain impact energy dependent fluence (of the order of 10^{21} m^{-2} at several keV/D exposures), after which D accumulation slowed down. This threshold fluence was estimated to correspond to the onset of D saturation in the implantation zone at a D/Be ratio of 0.3–0.4. The observed slow down of D accumulation coincided with the emergence of a distinct low-temperature desorption stage in TDS measurements, attributed by the authors to hydrogen adsorbed on porous surfaces and retained in molecular form in small bubbles formed in the material during ion implantation. Similar microstructure modifications were also observed by Yoshida et al. [7] who followed the evolution of Be microstructure by *in-situ* TEM during irradiation with

* Corresponding author.
E-mail address: d.matveev@fz-juelich.de (D. Matveev).

https://doi.org/10.1016/j.nme.2019.100682
Received 14 August 2018; Received in revised form 29 April 2019; Accepted 29 April 2019
Available online 03 May 2019

4 keV/D ions and subsequent isochronal annealing with 100 K steps.

In more recent works by Reinelt and Oberkofler [8,9], involving in particular single crystalline Be, experimental results in combination with results of density function theory (DFT) calculations [10] for hydrogen diffusion and trapping in single vacancies in Be served to setup a reaction-diffusion model describing fundamental processes of hydrogen interaction with beryllium. Experiments confirmed the slow down of D accumulation for the fluence of about 2×10^{21} m^{-2} at 1 keV/D, in agreement with earlier results for such implantation conditions by Haasz [11]. The initial reaction-diffusion model, called Coupled Reaction-Diffusion Systems (CRDS) code [9,12], could fairly well fit TDS profiles of low fluence implanted single crystalline Be, however could not explain the slow down of D accumulation and emergence of the low temperature release stage. The actual status of the CRDS code addressing the fluence dependence of hydrogen retention in beryllium is summarized in our previous work [13]. In the model, hydrogen retention under the threshold fluence is attributed to multiple-trapping in single vacancies, which tends to saturate with fluence. Hydrogen retention above the threshold fluence is attributed to formation of a modified morphology of the implantation zone, such as e.g. porous surfaces, represented in the model as an effective increased surface area where hydrogen isotopes can accumulate before temperature activated and surface coverage dependent desorption takes place. So far the model cannot address retention in form of gas bubbles.

Isotope-exchange experiments can give a further insight into the mechanisms of hydrogen transport and retention in materials. In particular, experiments and reaction-diffusion simulations for isotope-exchange in tungsten were very successful to confirm the multiple-trapping mechanism in vacancies [14,15]. In this paper we report the first, to our knowledge, isotope-exchange experiments on clean metallic Be under UHV laboratory conditions and respective CRDS modeling that gives a qualitative picture of possible processes involved. For that we developed a multi-isotope extension of the CRDS code. Due to particular uncertainties in the experimental data presented and discussed in Section 2, absolute comparison of the experiment and modeling is not possible. The model setup driven by experimental observations is described in Section 3. Simulation results are presented and discussed in Section 4.

2. Experimental

Isotope-exchange experiments were performed at Forschungszentrum Jülich in Germany. The experimental setup used is optimized for sample preparation, analysis and storage under UHV conditions with the base pressure of about 10^{-10} mbar, with capabilities of surface analysis using X-ray photo-electron spectroscopy (XPS), ultraviolet photo-electron spectroscopy (UPS), ion scattering spectroscopy (ISS), reflected electron energy loss spectroscopy (REELS) and thermal desorption spectroscopy (TDS). For the experiments two polycrystalline Be samples from the same batch were used. The sample size is 1.5 cm in diameter and 1 mm in thickness. Before each experimental run (implantation, analysis, TDS) the sample was sputter-cleaned and annealed at 900 K for 30 min, which was proven to have no legacy effects from the preceding exposure, also in agreement with experience in the past [8]. In the course of each experiment one Be sample was subject to the ion beam of one isotope until the desired exposure fluence has been accumulated, followed by exposure to the ion beam of the second isotope up to the same fluence, followed by thermal-desorption with a linear temperature ramp of 0.7 K/s. Exposures were done at room temperature. The resting times between exposures to the first and the second isotope and before TDS were of the order of several minutes. The direct (H followed by D) and reverse order (D followed by H) experiments, as well as only single isotope exposure experiments were carried out with the exposure fluence of $(1.0 - 5.5) \times 10^{21}$ m^{-2} for each isotope and the ion impact energy of 1500 eV/(H or D). The ion flux during exposures was of the order of 10^{18} m$^{-2}s^{-1}$. Direct and reverse order experiments will be referenced as H-D and D-H in the following. Sample cleaning, low base pressure in the vacuum chamber and restricted exposure times guarantee that the surface of the sample remains free from oxide layer during experiments as confirmed by the absence of the O-1s peak in XPS measurements at different stages. The conditions correspond, according to the literature [8], to the oxygen coverage of 0.2 monolayer or less. Thermal desorption spectra were recorded for masses 2 (H_2), 3 (HD) and 4 (D_2). Absolute calibration of the quadrupole mass spectrometer (QMS) could not be performed within this study due to technical reasons, so an assessment of the absolute isotope exchange efficacy remains outside of the scope of the present work. After the initial H-D experiment at a fluence of 5.5×10^{21} m^{-2} for each isotope, the sample holder and the secondary electron multiplier of the QMS had to be replaced, which resulted in a mismatch of the measured sample temperature of about 40 K and a change of the QMS sensitivity in the following D-H experiment at the same fluence. TDS spectra (as measured) for these experiments are presented in Fig. 1 (left for H-D and right for D-H). At $T > 800$ K a strong increase of the H_2 background due to outgassing from the sample holder and walls of the vacuum chamber is seen. In the case of the H-D spectra at $T < 350$ K an abnormal low-temperature peak of H_2 can be seen that at least partly can be attributed to the non-linearity of the temperature ramp at low temperatures and might be related to outgassing from the sample holder or even to degassing of the filament of the QMS. Further experiments with single isotope exposures (H only and D only) at different fluences were performed with the thermocouple spot-welded to the sample surface (before it was just clamped) and with QMS settings kept the same throughout the entire measurement series to ensure consistent temperature measurement and QMS signal intensities.

Measured TDS spectra for H only single isotope exposures at fluences 1.0×10^{21} m^{-2} and 5.5×10^{21} m^{-2} are shown in Fig. 2 (left). In addition the H_2 signal background during TDS measurement for D only exposure at a fluence of 1.0×10^{21} m^{-2} is shown that can be very well fitted with a double exponential growth function up to at least 1000 K, being consistent with H_2 spectra at $T > 850$ K from H only single isotope exposures. Such fitting is therefore used to remove the H_2 background from the TDS spectra of H implanted Be. In Fig. 2 (right) the H_2 and D_2 TDS spectra after H only and respectively D only single isotope exposures are shown together, with H_2 signals being corrected for the increasing background at higher temperatures as illustrated in Fig. 2 (left). From Fig. 2 the difference in H_2 and D_2 signal intensities becomes apparent. The difference between integrated H_2 and D_2 signals is a factor 3.7 for exposures at a fluence of 1.0×10^{21} m^{-2} (shaded areas in Fig. 2 (right)) and a factor 2.4 at a fluence of 5.5×10^{21} m^{-2}. Due to the lack of the absolute calibration, it is difficult to compare the total retained amounts of H and D. However, from earlier measurements by Oberkofler [9] and from the most recent measurements by Eichler [16] it is expected that deuterium retention is close to 100% for fluences below 10^{21} m^{-2}. Assuming that this holds for both H and D, the difference between integrated H_2 and D_2 signals for exposures at a fluence of 1.0×10^{21} m^{-2} must be due to different QMS sensitivities to H_2 and D_2. By conservatively setting the total retained amount equal in this case to 95% of the implanted amount [9] (the actual reflected fraction is less than 4% at 1500 eV according to simulations with the binary-collisions code SDTrimSP [17]) we can estimate the calibration factors for H and D signals. In such a way artificially post-calibrated TDS spectra from Fig. 2 (right) are shown in Fig. 3. It is interesting to note that using this post-calibration the total retention after exposures at a fluence of 5.5×10^{21} m^{-2} corresponds to about 39% and 62% of the implanted fluence for H and D exposures respectively. This may actually indicate that the slow down of H/D accumulation observed in earlier works, e.g. by Reinelt [8], Oberkofler [9] and Haasz [11], and attributed to the saturation of the high temperature peak in the TDS spectra, occurs probably earlier for H than for D. This is in line with the fact that already after a fluence of 1.0×10^{21} m^{-2} a small low temperature peak is

visible in the case of H. In our previous work [13] we demonstrate that the saturation may correspond to the situation where vacancy creation becomes balanced by vacancy annealing so that the total number of vacancies does not increase anymore and all vacancies become populated up to the maximal capacity by H or D atoms. Within this hypothesis the observation of earlier slow down of H accumulation can be probably related to the fact that H creates less Frenkel pairs (a vacancy and a self-interstitial Be atom) than D at the same impact energy. According to SDTrimSP simulations, at 1500 eV D produces approximately twice more recoils with energy above the displacement threshold (15 eV assumed here [18]) than H. From Fig. 3 it follows that the area under the high temperature peak increases after exposures at a fluence of 5.5×10^{21} m^{-2} compared to exposures at a fluence of 1.0×10^{21} m^{-2} by a factor of about 2. This, however, does not contradict the hypothesis of saturation of the number of produced vacancies. Although the number of vacancies does not increase anymore, the amount of retained H or D still can increase due to multiple trapping, so that more atoms occupy each vacancy. For a maximal occupancy of 5 atoms per vacancy according to DFT calculations [10,19] presumably achieved at a fluence of 5.5×10^{21} m^{-2}, we can then estimate that at a fluence of 1.0×10^{21} m^{-2} vacancies are occupied by ≈ 2.5 atoms in average. Another observation from Fig. 3 is that the high temperature peak is more extended to higher temperatures in the case of D, which can be also explained by slightly deeper penetration of D compared to H as also confirmed by SDTrimSP simulations (99% of implanted particles are stopped within 56.5 nm range in the case of H and within 63.5 nm range in the case of D). Finally, with the post-calibration imposed here, the low temperature peak for H appears to be significantly smaller than for D. It accounts for about 37% of the total retention against almost 50% in the case of D. This can be potentially also explained by the fact that by creating less damage H promotes less trapping sites with weaker binding, be it localized vacancy clusters or an extended modified surface area, e.g. due to interconnected porosity.

Unfortunately, the calibration factors estimated for single isotope exposures as described above cannot be applied to H-D and D-H experiments shown in Fig. 1 due to different settings of the QMS. For a very rough qualitative comparison of these experiments we shall assume the same ratio between QMS sensitivities for H_2 and D_2 in all experiments. Assuming in addition the QMS sensitivity to HD as the average of sensitivities to H_2 and D_2 and calculating the ratios of sensitivities H_2/D_2 and HD/D_2, we re-scale the H_2 and HD signals from Fig. 1. Finally we re-normalize the spectra assuming the same total amount of retained H and D (the total sum of H_2, D_2 and HD signals) in both experiments. We admit that we have no justification for this assumption and that the implantation order may have changed the total retained amount due to differences between H and D observed in single isotope exposures. Nevertheless, we hold this assumption as the most reasonable one to be able to compare H-D and D-H cases. The resulting spectra are shown in Fig. 4. It can be seen from Fig. 4 that isotope-exchange processes result in pronounced differences in the low temperature release stage where the second implanted isotope dominates. The effect is stronger in the case of the H-D exposure that can be also potentially attributed to the differences in damage creation by H and D described above. No significant differences between isotopes can be seen in the high temperature release stage, which means that both isotopes behave similarly in terms of trapping/de-trapping, being rather uniformly intermixed in vacancies with multiple trapping levels. Under the assumption that the number of created vacancies saturates at the threshold fluence during exposure to the first isotope, this observation indicates that the isotope exchange in vacancies is equally effective in both H-D and D-H experiments. However, in the absence of proper calibration, it is not really possible to distinguish the actual isotope exchange in already existing vacancies from additional vacancy creation by the second isotope. One may observe that D slightly dominates the high temperature release in the case of H-D exposure in the entire high temperature range (500 – 700 K), while in the case of D-H exposure, H dominates only in the range of 500 – 600 K, after which D takes over. This may serve as an indirect confirmation of the role of different implantation ranges of H and D. In the case of H-D, isotope exchange in vacancies is active through the entire depth affected by the first exposure to H. In the case of D-H, H cannot penetrate as deep as D so that isotope exchange in vacancies is less effective at the end of the implantation range of D.

3. Reaction-diffusion model

The CRDS code, presented in its latest modification in our previous work [13], has been further extended to allow simulations of two isotopes, H and D. The code takes into account the possibility of up to $n_{max} = 5$ (H + D) atoms occupying one vacancy, according to results of DFT computations [10,19]. The following system of 1D coupled partial differential equations describing the evolution of densities [m^{-3}] of hydrogen c_H, deuterium c_D and vacancies $c_{V_{ij}}$ ($i = 0..n_{max}$, $j = 0..n_{max} - i$) filled with i hydrogen and j deuterium atoms is considered:

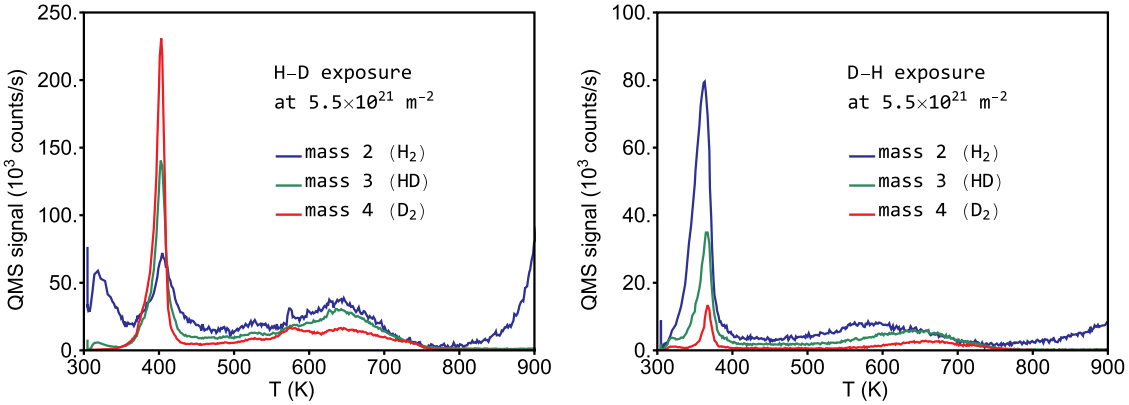

Fig. 1. TDS spectra recorded after 1500 eV H-D (left) and D-H (right) exposures at a fluence of 5.5×10^{21} m^{-2} for each isotope. The signals are not absolutely calibrated; the difference in signal intensities in two experiments is due to replacement of the secondary electron multiplier of the QMS between experiments. The $\approx$ 40 K shift of the position of the low temperature peak in the case of the D-H exposure is related to the change of the sample holder between experiments.

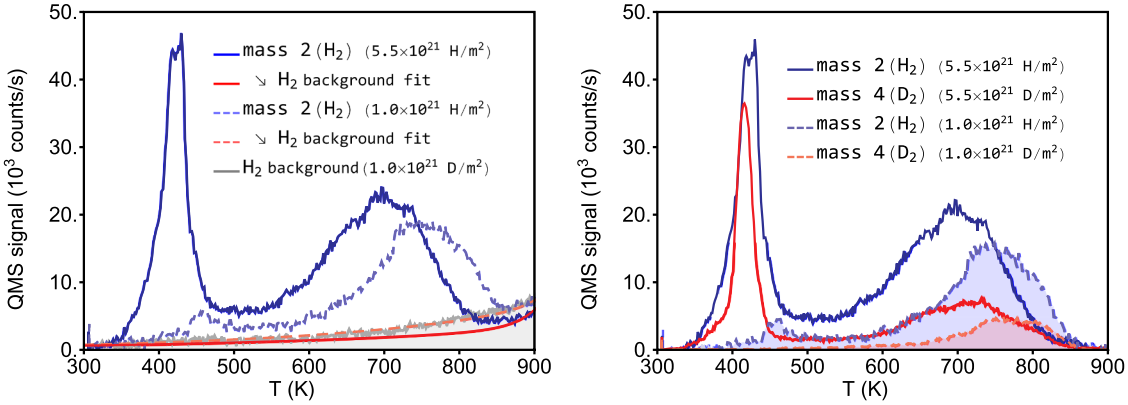

Fig. 2. TDS spectra (mass 2) recorded after 1500 eV single H isotope exposures at fluences of 1.0×10^{21} m^{-2} and 5.5×10^{21} m^{-2} (left). The H_2 signal background from a D only exposure TDS run is also shown fitted with a double exponential growth function. This signal illustrates the contribution of the H_2 background (not related to outgassing from the sample) to TDS spectra after single H exposures. TDS spectra (masses 2 and 4) recorded after 1500 eV single H and single D isotope exposures at fluences of 1.0×10^{21} m^{-2} and 5.5×10^{21} m^{-2} (right). The signals for mass 2 are corrected for the increasing H_2 background at higher temperatures as illustrated in the left figure.

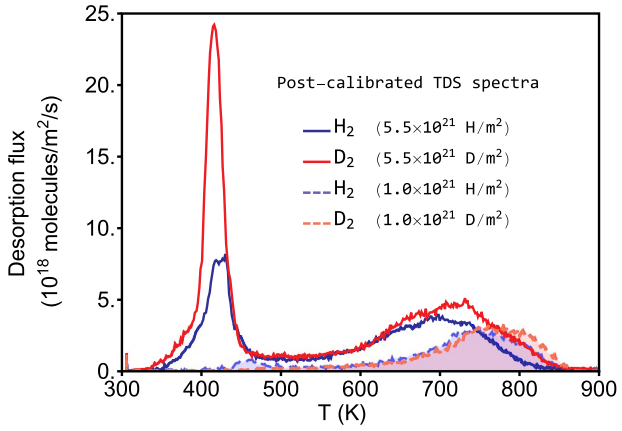

Fig. 3. TDS spectra from Fig. 2 (right) artificially post-calibrated assuming 95% retention after exposures at a fluence of 1.0×10^{21} m^{-2}.

$$
\begin{cases}
\partial_t c_{\mathrm{H}} = & S_{\mathrm{H}} + D_{\mathrm{H}} \partial^2_{xx} c_{\mathrm{H}} \\
& + \sum_{i=0}^{n_{\max}-1} \sum_{j=0}^{n_{\max}-i-1} \left(-R_{\mathrm{H}}^{\mathrm{tr,ij}} + R_{\mathrm{H}}^{\mathrm{dt,ij}} + R_{\mathrm{H}}^{\mathrm{kin,ij}}\right) \\
\partial_t c_{\mathrm{D}} = & S_{\mathrm{D}} + D_{\mathrm{D}} \partial^2_{xx} c_{\mathrm{D}} \\
& + \sum_{i=0}^{n_{\max}-1} \sum_{j=0}^{n_{\max}-i-1} \left(-R_{\mathrm{D}}^{\mathrm{tr,ij}} + R_{\mathrm{D}}^{\mathrm{dt,ij}} + R_{\mathrm{D}}^{\mathrm{kin,ij}}\right) \\
\partial_t c_{\mathrm{Vij}} = & S_{\mathrm{Vij}} + D_{\mathrm{Vij}} \partial^2_{xx} c_{\mathrm{Vij}} \\
& - R_{\mathrm{H}}^{\mathrm{tr,ij}} - R_{\mathrm{D}}^{\mathrm{tr,ij}} \\
& - R_{\mathrm{H}}^{\mathrm{dt,ij}} - R_{\mathrm{D}}^{\mathrm{dt,ij}} \\
& + R_{\mathrm{H}}^{\mathrm{tr,(i-1)j}} + R_{\mathrm{D}}^{\mathrm{tr,i(j-1)}} \\
& + R_{\mathrm{H}}^{\mathrm{dt,(i+1)j}} + R_{\mathrm{D}}^{\mathrm{dt,i(j+1)}} \\
& - R_{\mathrm{H}}^{\mathrm{kin,ij}} - R_{\mathrm{D}}^{\mathrm{kin,ij}}
\end{cases}
\tag{1}
$$

In Eq. (1) the coordinate x represents the direction into the bulk of the material, with $x = 0$ corresponding to the ion exposed surface and $x = L$ corresponding to the backside of the sample. All species potentially are allowed to diffuse along x with corresponding temperature dependent diffusion coefficients D_{H}, D_{D} and $D_{\mathrm{V_{ij}}}$ [m^{2}s^{-1}]. Trapping R^{tr} and de-trapping R^{dt} reactions [m^{-3}s^{-1}] change the local densities of H, D and vacancies $\mathrm{V_{ij}}$ with corresponding filling by H and D atoms. Trapping of an H or D atom is possible only for $\mathrm{V_{ij}}$ with $i + j < n_{\max}$. Upon trapping of one H atom, the vacancy $\mathrm{V_{ij}}$ becomes $V_{(i+1)j}$, respectively $V_{i(j+1)}$ for trapping of one D atom. De-trapping leads to corresponding decrease of indices to $i - 1$ and $j - 1$. All trapping and de-trapping reaction rate coefficients are given in form of Arrhenius expressions with a given activation energy barrier for each process. Trapping and de-trapping reactions represent sources and sinks for respective $c_{\mathrm{V_{ij}}}$. The kinetic de-trapping terms $R^{\mathrm{kin,ij}}$ are described later in the text. H, D and empty vacancies are provided to the model via the volumetric source terms $S_{\mathrm{H}}(x, t)$, $S_{\mathrm{D}}(x, t)$ and $S_{\mathrm{V_{ij}}}(x, t)(i = 0, j = 0)$ [m^{-3}s^{-1}] that correspond to depth profiles of implanted ions and recoil atoms and are described by Gaussian fit functions to respective SDTrimSP simulation results. Source terms $S_{\mathrm{V_{ij}}}$ are null for $i + j > 0$. Since the source terms are time dependent, both implantation phases (one for each isotope), relaxation times after each exposure and the subsequent TDS run are simulated in one go.

The surface model is extended to two isotopes as follows. The density [m^{-2}] of H and D on the surface, σ_{H} and σ_{D} respectively, change according to

$$
\begin{aligned}
\frac{d\sigma_{\mathrm{H}}(t)}{dt} &= j_{\mathrm{H}}^{\mathrm{bs}}(t) - 2j_{\mathrm{H_2}}^{\mathrm{des}}(t) - j_{\mathrm{HD}}^{\mathrm{des}}(t), \\
\frac{d\sigma_{\mathrm{D}}(t)}{dt} &= j_{\mathrm{D}}^{\mathrm{bs}}(t) - 2j_{\mathrm{D_2}}^{\mathrm{des}}(t) - j_{\mathrm{HD}}^{\mathrm{des}}(t).
\end{aligned}
\tag{2}
$$

The fluxes for bulk-surface transition $j^{\mathrm{bs}}(t)$ and desorption due to molecular recombination $j^{\mathrm{des}}(t)$ are given by

$$
j_{\mathrm{H}}^{\mathrm{bs}}(t) = K_{\mathrm{H}}^{\mathrm{bs}}\left(1 - \frac{\sigma_{\mathrm{H}}(t) + \sigma_{\mathrm{D}}(t)}{\sigma_{\max}}\right) c_{\mathrm{H}}(0, t),
\tag{3}
$$

$$
\begin{aligned}
j_{\mathrm{D}}^{\mathrm{bs}}(t) &= K_{\mathrm{D}}^{\mathrm{bs}}\left(1 - \frac{\sigma_{\mathrm{H}}(t) + \sigma_{\mathrm{D}}(t)}{\sigma_{\max}}\right) c_{\mathrm{D}}(0, t), \\
j_{\mathrm{H_2}}^{\mathrm{des}}(t) &= K^{\mathrm{rec}} \sigma_{\mathrm{H}}^2(t), \\
j_{\mathrm{D_2}}^{\mathrm{des}}(t) &= K^{\mathrm{rec}} \sigma_{\mathrm{D}}^2(t), \\
j_{\mathrm{HD}}^{\mathrm{des}}(t) &= K^{\mathrm{rec}} \sigma_{\mathrm{H}}(t) \sigma_{\mathrm{D}}(t).
\end{aligned}
\tag{4}
$$

The rate coefficients for the bulk-surface transition K^{bs} for H and D in Eq. (3) have an Arrhenius form with an activation energy assumed to be equal to the respective diffusion barrier. The surface occupation dependent factor is introduced so that the transition from the bulk to the surface takes place when there are a) H or D atoms available in the subsurface layer and b) empty sites available on the surface that can be occupied. Otherwise the flux from the bulk to the surface reduces to zero. The maximal density of surface sites shared by H and D atoms is given by $\sigma_{\max}$. Rate coefficients K^{rec} for molecular recombination in form of H_2, HD and D_2 in Eq. (4) are assumed to have the same surface occupation dependent activation energy $E_{\mathrm{des}}(\sigma)$ (Eq. (5)) to describe the

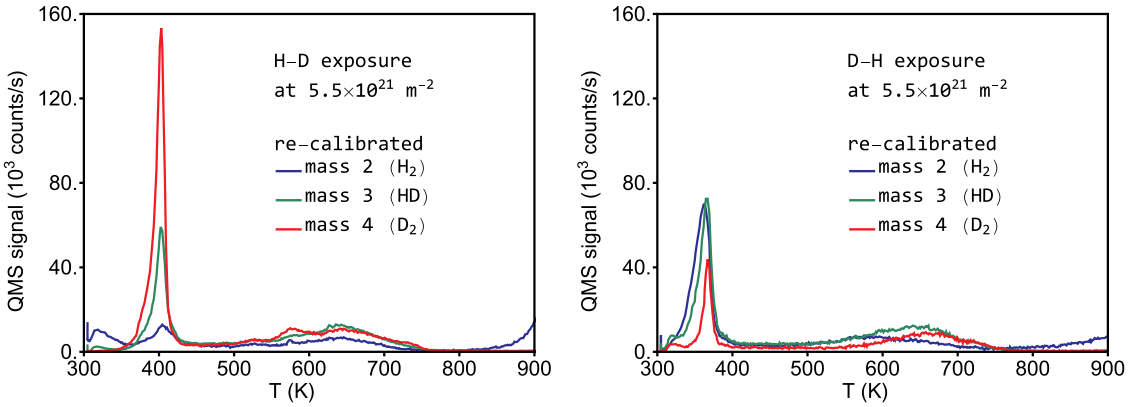

Fig. 4. TDS spectra from Fig. 1 re-scaled assuming the same ratio of QMS sensitivities to H_2 and D_2 as in single isotope exposures and re-normalized assuming the same total amount of retained H and D in both experiments. Contrary to Fig. 3, re-normalized QMS signals are plotted instead of absolute desorption fluxes since absolute calibration factors in these experiments must be different from single isotope exposures as described in Section 2.

barrier-free desorption above certain stable coverage configurations as can be expected from DFT simulations [20,21]. A rough or porous surface with an increased effective surface area is taken into account as described in [13].

$$E_{\mathrm{des}}(\sigma) = E^0_{\mathrm{des}}(1 - \exp(-\alpha(1 - \frac{\sigma_{\mathrm{H}} + \sigma_{\mathrm{D}}}{\sigma_{\mathrm{max}}})). \tag{5}$$

$E^0_{\mathrm{des}} = 1$ eV is the assumed undisturbed desorption barrier and α is a parameter defining the steepness of the transition to zero barrier around $\sigma_{\mathrm{H}} + \sigma_{\mathrm{D}} = \sigma_{\mathrm{max}}$ (we use $\alpha = 10$).

The initial condition for system (1) is an empty, vacancy-free sample, and boundary conditions equate the transition flux from the bulk to the surface j^{bs} and the diffusion flux from the bulk:

$$\partial_x c_{\mathrm{H}}(x, t)|_{x=0} = \frac{j^{\mathrm{bs}}_{\mathrm{H}}(t)|_{x=0}}{D_{\mathrm{H}}(T(t))},$$
$$\partial_x c_{\mathrm{D}}(x, t)|_{x=0} = \frac{j^{\mathrm{bs}}_{\mathrm{D}}(t)|_{x=0}}{D_{\mathrm{D}}(T(t))}. \tag{6}$$

As it was demonstrated in [13], the assumption of the saturation of the amount of vacancies in the sample with the fluence is essential to explain the observed fluence dependence of thermal desorption from single crystalline Be exposed to D ions. The same assumption is imposed here for simulations of isotope exchange experiments. This implies that for exposures at a fluence of 5.5×10^{21} m^{-2}, the saturation is reached already during exposure to the first isotope, so that all vacancies are filled by 5 atoms of that isotope and no atoms of the second implanted isotope can be trapped in vacancies, unless some isotope-exchange mechanism takes place. Simple de-trapping from the lower binding states in vacancies cannot be expected at room temperature, since the activation energy for these states is above 1 eV according to DFT [19]. A possible mechanism responsible for the isotope exchange in vacancies could be the kinetic de-trapping that has been also considered earlier for Be co-deposited layers by Kogut et al. [22]. The kinetic de-trapping terms $R^{\mathrm{kin,ij}}$ in Eq. (1) are given as in [22] by

$$R^{\mathrm{kin,ij}} = \sigma^{\mathrm{kin,ij}} J(x, t), \tag{7}$$

were σ^{kin} is the total cross-section for elastic collisions leading to sufficient energy transfer for de-trapping of an H (or D) atom by the impact of an H (or D atom), and the flux $J(x, t)$ [m^{-2}s^{-1}] represents the flux of implanted species that passes through a given point inside the material. To calculate $J(x_0, t)$ at a given point x_0, a simplified approach is used, in which the depth profile given by the respective source term $S(x, t)$ in Eq. (1) is integrated from $x = 0$ to $x = x_0$ and the result is subtracted from the total flux of implanted ions as in [22]. It has to be noted that, generally speaking, kinetic de-trapping should also affect H and D atoms trapped at open surfaces and would correspond to sputtering of surface atoms. We neglected the sputtering effect so far, since it results in similar depletion of the surface concentration as provided by the reduced desorption barrier at high coverages. Moreover, under the assumption of an increased surface area due to surface porosity, estimation of sputtering yields and accounting for re-deposition of sputtered atoms inside the pores becomes non-trivial.

Thus the following isotope-exchange mechanisms can be modeled:

- Kinetic de-trapping leads to de-trapping of first implanted isotope from saturated vacancies. The emptied trapping levels can be occupied from the solute population of one or another isotope. This mechanism affects the high temperature release stage but also provides additional atoms to the surface.
- Surface coverage dependent desorption barrier allows desorption even at room temperature at near-saturation surface coverages. If surface saturation is reached during exposure to the first isotope, molecules of the first isotope will desorb during the second implantation. This will again lead to predominance of the second implanted isotope in the surface reservoir. Only the low temperature desorption stage is thus affected.

The diffusion coefficients D_H and D_D are assumed to be inversely proportional to the square root of the atomic mass of the isotope. We use the same parameters for D diffusion as in our work [13] and respectively corrected by the square root of the mass ratio value for H. Trapping and de-trapping parameter are also taken over from that work with activation energies for de-trapping being equal to 1.5 eV for the first 3 atoms in a vacancy and 1.3 eV for the additional two, which showed rather good agreement with the shape of the high temperature TDS peak in experiments with Be single crystals [8].

The dynamics of vacancies during ion irradiation, namely their creation, diffusion to sinks such as grain boundaries, annihilation with self-interstitial Be atoms and clustering, is probably responsible for saturation of vacancies with hydrogen isotopes and appearance of the low temperature release peak. Despite single vacancy dynamics can be in principle simulated within the reaction-diffusion approach, here we adopt the simple assumption from our previous work [13] that a certain fraction ξ of vacancies produced by ion irradiation survives annihilation with self-interstitial Be atoms up to the point when the threshold implantation fluence is reached. When the threshold fluence of 1.0×10^{21} m^{-2} is accumulated, ξ is set to zero. This way for sufficiently large ξ in the beginning of exposure vacancies are filled by less than n_{max} (H + D) atoms. We choose $\xi_{\mathrm{H}} = 1/15$ for H and $\xi_{\mathrm{D}} = 1/30$ for D so that approximately one vacancy survives in average (over the implantation zone) per 3 incident H or D to reflect the approximate vacancy occupancy at a fluence of 1.0×10^{21} m^{-2} as estimated from the experimental data in Section 2. As in our earlier work [13] we

neglected the vacancy diffusion. After the threshold fluence is reached, vacancy creation is switched off and the accumulated vacancies are further populated up to the saturation to $n_{max} = 5$ (H + D) atoms. From this point the newly implanted atoms and those that are kinetically de-trapped from vacancies can diffuse and occupy open surfaces with an extended surface area. When the total surface density of H and D atoms approaches the saturation value σ_{max}, the desorption energy barrier reduces so that desorption at room temperature takes place. The emptied surface sites can be then further occupied by solute H and D atoms. As it was shown in Section 2, the low temperature peak after high fluence single isotope exposures is higher in the case of D (Fig. 3), therefore we assume that D, by creating more damage, promotes more low energy trapping sites. To account for this hypothetical effect, we impose different effective surface areas for H and for D. From the total amounts of retained H and D corresponding to low temperature peaks in Fig. 3 at a fluence of 5.5×10^{21} m^{-2}, assuming that this retention is attributed to the extended surfaces, we can estimate how much the effective surface area has to exceed the nominal surface area. We use here the nominal maximal surface concentration of 2.22×10^{19} m^{-2}, which results in approximately 40 times larger surface area needed in the case of H exposure and respectively about 80 times larger area needed in the case of D exposure. Therefore these values are used in the simulations. Interestingly, this factor 2 difference reflects the approximate ratio between damage created in Be by D and H respectively according to SDTrimSP simulations. We would like to stress that this is just an approach to describe the low temperature release stage in our 1D reaction-diffusion simulations [13]. In reality the retention above the threshold fluence might be related to formation of gas filled bubbles and blisters as suggested by earlier works of Chernikov and colleagues [4], as well as by the most recent results of Eichler [16], that would require an assessment of the initial vacancy cluster formation. Larger surface area can be also seen as surface porosity, and in the context of this work, the factor how much the surface area used in the simulation is increased compared to the nominal surface area is just a parameter proportional to the density of low energy trapping sites of whatever nature. Although in this case it can be expected that this parameter has to be fluence dependent, we use a simplified approach and assume that the surface area is constant throughout the simulation, except for the case of the H-D experiment, where we instantaneously increase the surface area at the beginning of D exposure. In the case of the D-H experiment, we assume that the surface area corresponds to that of D and does not change with H exposure.

4. Simulation results

Results of simulations with the above described setup for single isotope exposures and direct and reversed isotope-exchange experiments are shown in Figs. 5–7.

Fig. 5 has to be compared to Fig. 3 and shows simulated TDS spectra after single isotope exposures at different fluences. As in experiments, the change of the spectra with fluence is reproduced, namely the growth and broadening of the high temperature peak due to multiple-trapping and appearance of the low temperature peak due to H/D accumulation on the surface. The exact shape of the high temperature peak depends on properties of trapping of multiple atoms in single vacancies, diffusion properties of hydrogen isotopes and, in particular, the role of grain boundaries, which was neglected in the modeling. The narrow width of the low temperature peak cannot be reproduced under standard assumptions of molecular desorption as we have already mentioned in [13]. Simulated low temperature peaks are broader and therefore lower than in the experiments (Fig. 3). As an approximation, however, our assumptions catch the qualitative dependencies correctly. Due to twice larger effective surface area assumed for D, the low temperature peak is higher in the case of D after the high fluence exposure. This can be also seen in the integral retained amounts of H and D, which account for 49% and 62% of the implanted fluence compared to 39%

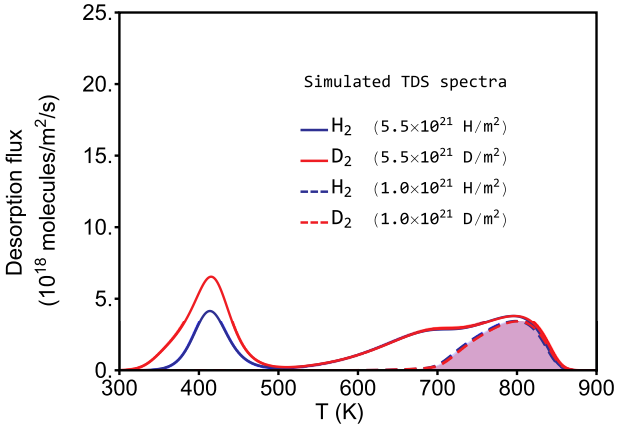

Fig. 5. Simulated TDS spectra for single isotope exposures at fluences of 1.0×10^{21} m^{-2} and 5.5×10^{21} m^{-2}.

and 62% estimated from the experimental data. Keeping in mind all the uncertainties with experimental determination of the retained fraction, we obtained good qualitative agreement between experiments and modeling.

Fig. 6 has to be compared to Fig. 4 and shows simulated TDS spectra after H-D and D-H experiments. Here we note that H and D dominate the high temperature release stage when they were implanted the last, which is attributed to overestimated cross-section of kinetic de-trapping. Minor differences in the shape of the high temperature peak for H and D can be attributed to slightly different depth profiles of implanted ions and 10% difference in the kinetic de-trapping cross-sections σ_{kin} for H-H, H-D, D-H and D-D collisions that we imposed due to differences in masses of colliding nuclei ($\sigma_{H-H} = \sigma_{D-D} = 0.250 \times 10^{-20}$ m^2, $\sigma_{H-D} = \sigma_{D-H} = 0.225 \times 10^{-20}$ m^2). The pronounced dominance of the second implanted isotope in the low temperature release stage is reproduced, although the H-D (left) and D-H (right) cases appear to be symmetric contrary to the experiment where the difference between isotopes is more pronounced in the case of H-D (Fig. 4). This is despite twice larger effective surface area assumed in the model under the impact of D ions. We explain it by the fact that we assumed immediate increase of the effective surface area at the beginning of the second implantation in the case of the H-D experiment that led to immediate reduction of the surface coverage by factor 2 and prevented H desorption due to surface saturation.

Fig. 7 illustrates the evolution of surface concentrations of H and D during simulations for H-D (left) and D-H (right) experiments. Surface concentrations are normalized to the maximal surface concentration. The drop of H concentration at the beginning of D exposure in the H-D experiment is explained by the instantaneous increase of the surface area imposed in the model, and the subsequent increase of H concentration is due to kinetically de-trapped H diffusing to the surface. Although vacancy production is switched off at $t = 1000$ s (at an implanted fluence of 1.0×10^{21} m^{-2}), the surface concentration of the first implanted isotope starts to grow only from about $t = 2000$ s since it takes time until all vacancies get populated up to the maximal capacity and the excess solute atoms reach the surface. Imposing earlier saturation of vacancy production would not change the qualitative picture of the processes taking place.

5. Conclusion

Results of first to our knowledge H/D isotope-exchange experiments on Be under UHV laboratory conditions have been presented. TDS measurements for experiments at equal fluences for both isotopes indicate that isotope exchange takes place leading to comparable release of both isotopes in the high temperature part of TDS spectra, while the last implanted isotope dominates the release during the low

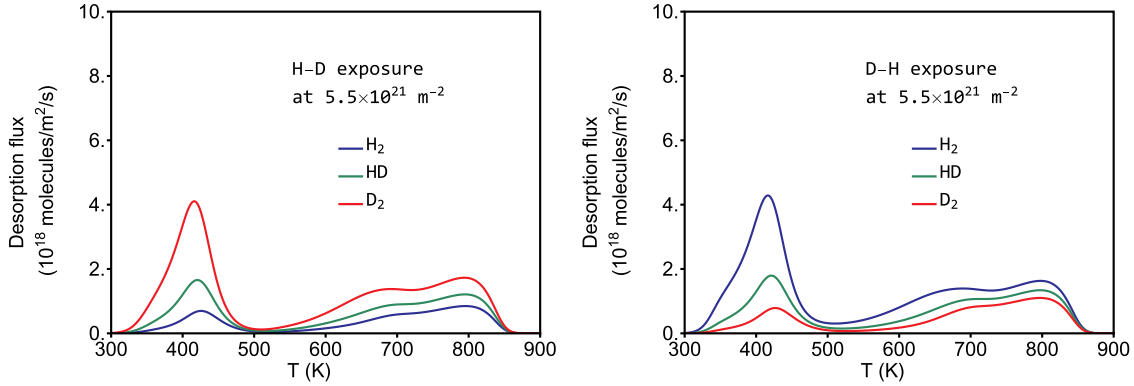

Fig. 6. Simulated TDS spectra for H-D (left) and D-H (right) experiments at a fluence of 5.5×10^{21} m^{-2} for each isotope.

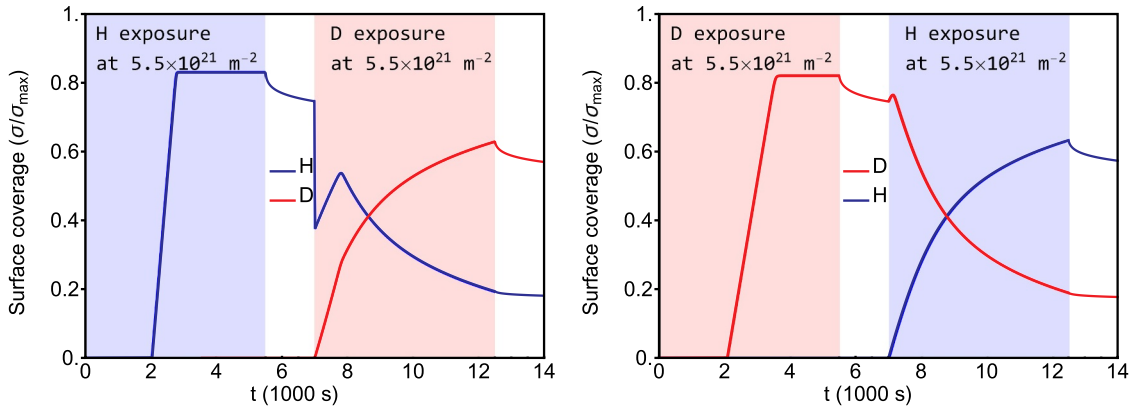

Fig. 7. Simulated evolution of surface concentrations of H and D in H-D (left) and D-H (right) experiments at a fluence of 5.5×10^{21} m^{-2} for each isotope. The time intervals with H or D implantation are shaded. The relaxation time intervals between two isotopes exposures and before TDS are set to 1500 s. The drop of the H concentration at the beginning of the D exposure in the H-D experiment is explained by the instantaneous increase of the surface area imposed in the model, and the subsequent increase of the H concentration is due to kinetically de-trapped H diffusing to the surface.

temperature release stage. A reaction-diffusion model has been presented that can treat hydrogen and deuterium transport and trapping in crystalline beryllium taking into account multiple mixed (H + D) trapping in single vacancies, kinetic de-trapping during ion irradiation and H and D accumulation on an extended surface area representing low energy trapping sites with occupation dependent desorption as an approach to describe H/D retention due to modified surface morphology, e.g. formation of gas bubbles and development of surface porosity. Simulation results suggest the applicability of the model to describe isotope exchange processes in crystalline beryllium and give a qualitative explanation of the observed experimental facts. The fluence dependence of retention for H and D is governed by a) vacancy creation due to ion impact at low fluences; b) saturation of the number of created vacancies in the implantation zone when a certain threshold fluence is reached; c) population of available vacancies by H and D up to the maximal occupancy of 5 atoms per vacancy; d) accumulation of the excess amount of implanted atoms on open surfaces, e.g. interconnected porosity; e) barrier-free molecular recombination at near-saturation surface coverage. Isotope exchange in vacancies is driven by kinetic de-trapping of already trapped atoms and re-trapping of solute atoms of both isotopes in vacancies with multiple trapping levels resulting in rather comparable presence of both isotopes in the high temperature desorption stage. The predominance of the second implanted isotope in the low temperature desorption stage is attributed to predominant molecular desorption of the first implanted isotope from the saturated surface with simultaneous predominant repletion of the surface population by the second implanted isotope during the second exposure. Quantitative comparison to experimental data is not possible due to the lack of absolute calibration of the TDS system and the forced necessity to replace the sample holder and the electron multiplier of the QMS between different experimental runs. Detailed and better controlled experiments are necessary to further adjust the parameters of the model. Exposures varying the fluence and energy separately for each isotope within one experiment could be of interest to reveal the dynamics of isotope-exchange processes at low energy and high energy trapping sites.

Acknowledgement

This work has been carried out within the framework of the EUROfusion Consortium and has received funding from the Euratom research and training programme 2014–2018 under grant agreement No 633053. This work was performed within the EUROfusion work package PFC. The views and opinions expressed herein do not necessarily reflect those of the European Commission.

References

[1] G. Federici, R. Doerner, P. Lorenzetto, V. Barabash, Compr. Nucl. Mater. 4 (2012) 621–666. Chapter 4.19
[2] R. Anderl, R. Causey, J. Davis, et al., J. Nucl. Mater. 273 (1999) 1.
[3] R. Causey, J. Nucl. Mater. 300 (2002) 91.
[4] V.N. Chernikov, V.K. Alimov, A.V. Markin, A.E. Gorodetsky, S.L. Kanashenko, A.P. Zakharov, I.B. Kupriyanov, J. Nucl. Mater. 233–237 (1996) 860–864.
[5] A. Markin, V. Chernikov, S. Rybakov, A. Zakharov, J. Nucl. Mater. 233–237 (1996) 865–869.
[6] V.K. Alimov, V.N. Chernikov, A.P. Zakharov, J. nucl. mat. 241–243 (1997) 1047–1052.
[7] N. Yoshida, S. Mizusawa, R. Sakamoto, T. Muroga, J. Nucl. Mater. 233–237 (1996) 874–879.
[8] M. Reinelt, A. Allouche, M. Oberkofler, C. Linsmeier, New J. Phys. 11 (2009)

043023.
[9] M. Oberkofler, M. Reinelt, C. Linsmeier, Nucl. Instr. Meth. B 269 (2011) 1266.
[10] A. Allouche, M. Oberkofler, M. Reinelt, C. Linsmeier, J. Phys. Chem. C 114 (2010) 3588.
[11] A. Haasz, J. Davis, J. Nucl. Mater. 241–243 (1997) 1076.
[12] R. Piechoczek, M. Reinelt, M. Oberkofler, A. Allouche, C. Linsmeier, J. Nucl. Mater. 438 (2013) S1072.
[13] D. Matveev, et al., Nucl. Instr. Methods Phys. Res. B 430 (2018) 23.
[14] K. Schmid, U. von Toussaint, T. Schwarz-Selinger, J. Appl. Phys. 116 (2014) 134901.
[15] J. Bauer, T. Schwarz-Selinger, K. Schmid, These proceedings.
[16] M. Eichler, et al., Nucl. Mater. Energy 19 (2019) 440.
[17] W. Eckstein, R. Dohmen, A. Mutzke, R. Schneider, SDTrimSP: a monte-carlo code for calculating collision phenomena in randomized targets, IPP Rep. 12/3 (2007) 621–666. For Fission and Fusion Reactors, (2012), p. Elsevier Reference Module in Materials Science and Materials Engineering
[18] P.V. Vladimirov, V.A. Borodin, Nucl. Instr. Methods Phys. Res. B 393 (2017) 195.
[19] L. Ferry, et al., Tritium behaviour in beryllium investigated by DFT, Presented at the 16th international conference on plasma-facing materials and components, 16–19, Neuss (Germany), (2017).
[20] Ch. Stihl, Recent progress in DFT based multi-scale modeling of hydrogen interactions with beryllium (0001) surfaces, Presented at the Third 4 International Workshop on Models and Data for Plasma-Material Interaction in Fusion Devices, 22–24, Jülich (Germany), (2017).
[21] Z. Piazza, M. Ajmalghan, Y. Ferro, R.D. Kolasinski, Acta Materialia 145 (2018) 388.
[22] D. Kogut, et al., Phys. Scr. T167 (2016) 014062.